Enhancement of dilepton production rate and electric conductivity around QCD critical point

Toru Nishimura^{1,2}, Masakiyo Kitazawa^{2,3,1}, and Teiji Kunihiro²

¹Department of Physics, Osaka University, Toyonaka, Osaka, 560-0043

Japan

*E-mail: nishimura@kern.phys.sci.osaka-u.ac.jp

² Yukawa Institute for Theoretical Physics, Kyoto University, Kyoto,
606-8502 Japan

³J-PARC Branch, KEK Theory Center, Institute of Particle and Nuclear Studies, KEK, 319-1106 Japan

We investigate whether the soft mode that becomes massless at the QCD critical point (CP) causes an enhancement of the dilepton production rate (DPR) and the electric conductivity around the CP through the modification of the photon self-energy. The modification is described by the so-called Aslamazov-Larkin, Maki-Thompson and density of states terms, which have been taken into account in our previous study on the DPR near the color-superconducting phase transition, with a replacement of the diquark modes with the soft mode of the QCD CP. We show that the coupling of photons with the soft modes brings about an enhancement of the DPR in the low invariant-mass region and the conductivity near the CP, which would be observable in the relativistic heavy-ion collisions.

1 Introduction

Exploring the high-density matter at vanishing and finite temperature in Quantum Chromodynamics (QCD) is one of the most challenging as well as intriguing subjects in the current nuclear physics [1]. Among various interesting subjects, the possible existence of a critical point called the QCD CP on the QCD phase diagram has been acquiring much attention. The phase transition at the QCD CP is of second order with the same universality class as the Z_2 Ising model, and large fluctuations of various quantities coupled to the order parameter are expected to occur [2, 3]. A number of proposals have been made for observational identification of the QCD CP in the relativistic heavy-ion collision (HIC) experiments [1–8], such as the event-by-event fluctuations of conserved charges and especially their non-Gaussianity, large fluctuations of the low-momentum particle distributions, anomalous fluid dynamical phenomena with diverging transport coefficients and so on. Active experimental analyses are ongoing at the beam-energy scan program at RHIC, NA61/SHINE, and HADES [9]. The future experiments at FAIR and J-PARC-HI will further pursue them [10, 11].

In this article, we investigate possible signals of the QCD CP that would be observed in these experiments on the basis of the fact that the second-order nature of the QCD CP implies the existence of a low-energy mode with a vanishing mass at the CP. Such a slow mode is called the soft mode of the phase transition. The soft mode of the QCD CP is fluctuations in the scalar channel but *not* a sigma *mesonic* mode. Instead, it is the particle-hole (p-h) collective excitation with a mixing of baryon number density and energy density that has a spectral support in the space-like region [12–15].

The existence of the soft mode should affect various observables near the CP. In this article, as examples of such observables, we explore how the dilepton production rate (DPR) and the electric conductivity are affected by the soft mode of the QCD CP. We have shown in a previous work Ref. [16] that the DPR can be greatly enhanced in the low invariant-mass region near the phase boundary of the two-flavor color superconductivity (2SC) due to the diquark soft mode [17–20]; in Ref. [16], the enhancement of the DPR originates from a modification of the photon self-energy by the Aslamazov-Larkin (AL) [21], Maki-Thompson [22, 23] and density of states (DOS) terms [24] incorporating the diquark soft modes. A surprise in Ref. [16] was that although the spectral support of the diquark soft mode is concentrated in the space-like region, their scattering process described by the AL term does cause the enhancement of the DPR in the time-like region. We thus expect that such an enhancement of these observables may occur by a similar mechanism due to the soft mode associated with the QCD CP; we consider the AL, MT and DOS terms with

the diquark soft modes being replaced by the soft mode of the QCD CP in the 2-flavor Nambu–Jona-Lasinio (NJL) model.

A notable feature of the soft mode of the QCD CP is that its propagator is not analytic at the origin unlike the diquark modes investigated in Ref. [16]. As a result, a simple time-dependent Ginzburg-Landau (TDGL) approximation is not applicable to describe the soft mode of the QCD CP. We thus introduce an approximation scheme that simply takes care of the specific analytic properties. The vertex functions in the AL, MT and DOS terms are then constructed so as to be consistent with this treatment in light of the gauge invariance. In this way, our photon self-energy is constructed to satisfy the Ward-Takahashi (WT) identity.

Using the photon self-energy thus constructed, we calculate the DPR and the electric conductivity near the QCD CP. We show that the DPR at low invariant-mass region, as well as the electric conductivity, is greatly enhanced around the QCD CP due to the soft modes. We also present some issues which are relevant when pursuing an experimental measurement of these signals in the HIC experiments.

This paper is organized as follows. In the next section, after introducing the model and its phase diagram in the mean-field approximation, we discuss properties of the soft mode of the QCD CP. In Sec. 3, we calculate the photon self-energy described by the AL, MT and DOS terms. In Sec. 4, we discuss the numerical results on the DPR and the electric conductivity near the QCD CP. The final section will be devoted to a short summary.

2 Phase diagram and soft modes of QCD CP

To investigate the DPR and electric conductivity near the QCD CP, we adopt the following 2-flavor NJL model [25]

$$\mathcal{L} = \bar{\psi}i(\partial \!\!\!/ - m)\psi + G_S[(\bar{\psi}\psi)^2 + (\bar{\psi}i\gamma_5\vec{\tau}\psi)^2], \tag{1}$$

where ψ is the quark field and $\vec{\tau} = (\tau_1, \tau_2, \tau_3)$ is the Pauli matrices for the flavor $SU(2)_f$. The current quark mass m = 5.5 MeV, the scalar coupling constant $G_S = 5.50$ GeV⁻² and the three-momentum cutoff $\Lambda = 631$ MeV are determined so as to reproduce the pion mass $m_{\pi} = 138$ MeV and the pion decay constant $f_{\pi} = 93$ MeV [25].

In Fig. 1, we show the phase diagram as a function of the temperature T and the quark chemical potential μ in the mean-field approximation with the mean field $\langle \bar{\psi}\psi \rangle$. The solid line shows the first-order critical line, and the circle marker denotes the QCD CP, which is located at $(T_c, \mu_c) \simeq (46.757, 329.30)$ MeV.

The soft mode of the QCD CP is described by the collective excitations of the scalar field $\bar{\psi}\psi$ [12, 26]. The imaginary-time Green's function of this channel in the random-phase

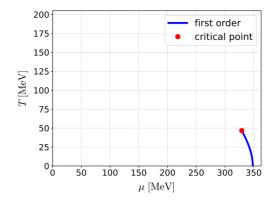


Fig. 1: Phase diagram calculated by the mean-field approximation in the 2-flavor NJL model (1). The solid line shows the first-order phase transition. The QCD CP is represented by the circle marker, which is located at $(T_c, \mu_c) \simeq (46.757, 329.30)$ MeV.

approximation (RPA) is given by [25]

$$\tilde{\Xi}(k) = \frac{1}{G_S^{-1} + \mathcal{Q}(k)},\tag{2}$$

$$Q(k) = 2N_f N_c \int_p \text{Tr}[\mathcal{G}_0(p-k)\mathcal{G}_0(p)], \qquad (3)$$

where $N_f = 2$ and $N_c = 3$ are the numbers of flavor and color, $\mathcal{Q}(k) = \mathcal{Q}(\boldsymbol{k}, i\nu_n)$ is the one-loop quark-anti-quark correlation function, $\mathcal{G}_0(p) = \mathcal{G}_0(\boldsymbol{p}, i\omega_m) = 1/[(i\omega_m + \mu)\gamma_0 - \boldsymbol{p} \cdot \boldsymbol{\gamma} + M]$ is the free-quark propagator, ω_m (ν_n) is the Matsubara frequency for fermions (bosons), $M = m - 2G_S\langle\bar{\psi}\psi\rangle$ is the constituent quark mass and Tr is the trace over the Dirac indices. Throughout this paper, we denote the momentum integration and Matsubara-frequency summation as $\int_p = T \sum_m \int d^3\boldsymbol{p}/(2\pi)^3$. The Green's function $\tilde{\Xi}(k)$ is represented by a sum of repeated bubble diagrams composed of the one-loop correlation function (3).

The retarded functions $\Xi^R(\mathbf{k},\omega)$ and $Q^R(\mathbf{k},\omega)$ corresponding to $\tilde{\Xi}(k)$ and Q(k) are obtained by an analytic continuation $i\nu_n \to \omega + i\eta$. The analytic formula of the imaginary

part of $Q^R(\mathbf{k},\omega)$ is calculated to be

$$\operatorname{Im} Q^{R}(\boldsymbol{k},\omega) = -\frac{N_{f}N_{c}T}{4\pi} \frac{\omega^{2} - \boldsymbol{k}^{2} - 4M^{2}}{|\boldsymbol{k}|} \times \left\{ \theta\left(|\omega| - \sqrt{\boldsymbol{k}^{2} + 4M^{2}}\right) F\left(\omega, \bar{k}(|\boldsymbol{k}|, \omega)\right) + \theta\left(\bar{k}(|\boldsymbol{k}|, \bar{\Lambda}) - |\omega|\right) \left[F\left(\omega, \bar{k}(|\boldsymbol{k}|, \omega)\right) - F\left(\omega, \bar{\Lambda}\right) \right] \right\},$$
(4)

$$F(\omega, x) = \sum_{s,t=\pm} s \log \cosh \frac{\omega + sx - 2t\mu}{4T},$$
 (5)

$$\bar{k}(|\mathbf{k}|,\omega) = |\mathbf{k}|\sqrt{1 - 4M^2/(\omega^2 - \mathbf{k}^2)}, \quad \bar{\Lambda} = 2\sqrt{\Lambda^2 + M^2},$$
 (6)

where $\bar{k}(|\mathbf{k}|, \bar{\Lambda}) < |\mathbf{k}|$. Then the real part is given by the Kramers-Kronig relation

$$\operatorname{Re}Q^{R}(\boldsymbol{k},\omega) = \frac{1}{\pi} P \int_{-\bar{\Lambda}}^{\bar{\Lambda}} d\omega' \frac{\operatorname{Im}Q^{R}(\boldsymbol{k},\omega')}{\omega' - \omega},\tag{7}$$

where P denotes the principal value.

The first and second terms in the curly bracket in Eq. (4) take nonzero values in the timeand space-like regions, respectively. $\Xi^R(\mathbf{k},\omega)$ has poles that physically represent collective modes in the time- and space-like regions, respectively. The former corresponds to the sigma meson composed of quark-anti-quark excitations, while the latter to that composed of p-h excitations due to the existence of a Fermi sphere.

From Eq. (4) one also finds that $Q^R(\mathbf{k}, \omega)$ is not analytic at the origin $(|\mathbf{k}|, \omega) = (0, 0)$. In fact, the limiting value of $\text{Im}Q^R(\mathbf{k}, \omega)$ at the origin along the line $\omega = a|\mathbf{k}|$ is given by

$$\lim_{|\mathbf{k}| \to 0} \operatorname{Im} Q^{R}(\mathbf{k}, a|\mathbf{k}|) = a \frac{N_{f} N_{c} M^{2}}{2\pi} \sum_{t=\pm} \left\{ \tanh \frac{\lambda_{0} - 2t\mu}{4T} - \tanh \frac{\bar{\Lambda} - 2t\mu}{4T} \right\} \theta \left(\frac{2\Lambda}{\bar{\Lambda}} - |a| \right), \quad (8)$$

with $\lambda_0 = \sqrt{4M^2/(1-a^2)}$. Equation (8) is nonzero for $0 < |a| < 2\Lambda/\bar{\Lambda} < 1$, in which the value depends on a.

At the QCD CP, $\Xi^{R}(\mathbf{k},\omega)$ satisfies

$$\Xi^{R^{-1}}(\mathbf{0},0)\big|_{T=T_c,\ \mu=\mu_c}=0,$$
 (9)

in accordance with the nature of the second-order phase transition at the CP. In fact, Eq. (9), known as the Thouless criterion [27], is derived from the stationary condition of the effective potential at the CP. The Thouless criterion shows the existence of a collective mode that becomes exactly massless in $\Xi^{R}(\mathbf{k},\omega)$. This mode is called the soft mode associated with the

CP. It is known that the soft mode of the QCD CP is a p-h mode in the space-like region, while the mesonic mode in the time-like region does not become massless even at the QCD CP [12, 14, 15, 26].

In the next section, we investigate the effect of the soft mode on the photon self-energy in the low energy and momentum region. For this analysis we introduce an approximate formula of $\Xi^R(\mathbf{k},\omega)$ that is valid near the QCD CP in the following way: First, since the spectral function of the soft mode has the support in the space-like region, we focus on the strength in the space-like region only. The mesonic mode in the time-like region is neglected since its contribution to the photon self-energy at low energy-momentum is suppressed because of the dispersion relation $\omega > \sqrt{\mathbf{k}^2 + 4M^2}$, where $M \simeq 185$ MeV around the CP. Second, we approximate the denominator of $\Xi^R(\mathbf{k},\omega)$ in the space-like region by expanding it with respect to ω and picking up the first two terms as

$$\Xi^{R}(\mathbf{k},\omega) = \frac{1}{G_{S}^{-1} + Q^{R}(\mathbf{k},\omega)} \sim \frac{1}{A(\mathbf{k}) + C(\mathbf{k})\omega},$$
(10)

where $A(\mathbf{k}) = G_S^{-1} + Q^R(\mathbf{k}, 0)$ and $C(\mathbf{k}) = \partial Q^R(\mathbf{k}, \omega)/\partial \omega \mid_{\omega=0}$, which are found to be real and pure-imaginary numbers, respectively, from Eqs. (4) and (7). We then write the imaginary part of Eq. (10) as

$$\operatorname{Im}\Xi^{R}(\boldsymbol{k},\omega) \sim \operatorname{Im}\frac{1}{A(\boldsymbol{k}) + C(\boldsymbol{k})\omega} \theta(\bar{k}(|\boldsymbol{k}|,\bar{\Lambda}) - |\omega|), \tag{11}$$

where we have used the fact that $\operatorname{Im}\Xi^R(\boldsymbol{k},\omega)$ takes a nonzero value for $|\omega| < \bar{k}(|\boldsymbol{k}|,\bar{\Lambda})$ in the space-like region, as seen from Eq. (4). In the next section, we use the forms of $A(\boldsymbol{k})$ and $C(\boldsymbol{k})$ determined in the NJL model for a given T and μ . It is shown that $C(\boldsymbol{k})$ behaves as $1/|\boldsymbol{k}|$ and diverges in the limit $|\boldsymbol{k}| \to 0$ corresponding to the non-analytic nature of $\Xi^R(\boldsymbol{k},\omega)$ at the origin. From this behavior a simple time-dependent Ginzburg-Landau (TDGL) approximation [24] that expands $[\Xi^R(\boldsymbol{k},\omega)]^{-1}$ with respect to ω and $|\boldsymbol{k}|$ is not applicable in the present case. Our approximation (11) is valid even in this case since the \boldsymbol{k} dependence is treated exactly. We also note that the denominator of Eq. (11) does not diverge at the origin since the term $C(\boldsymbol{k})\omega$ is suppressed by the condition $|\omega| < |\boldsymbol{k}|$ for $\boldsymbol{k} \to 0$.

To demonstrate the validity of Eq. (11), we show in Fig. 2 the contour maps of the dynamical structure factor given by

$$S(\mathbf{k}, \omega) = \frac{1}{\pi} \frac{1}{1 - e^{-\omega/T}} \operatorname{Im}\Xi^{R}(\mathbf{k}, \omega), \tag{12}$$

in the space-like region at and slightly away from the CP $(T = 0.9T_c, 1.0T_c \text{ and } 1.1T_c \text{ at } \mu = \mu_c)$. In each panel, the left and right subpanels are the results of the RPA, Eq. (2)

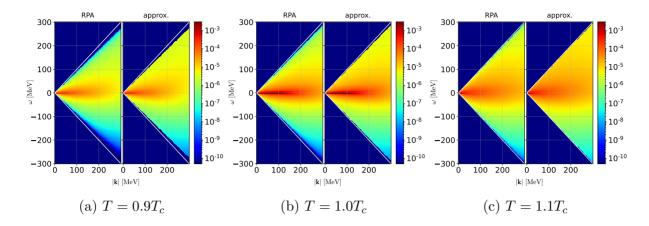


Fig. 2: Color maps of the dynamical structure factor $S(\mathbf{k}, \omega)$ in the space-like region for $T = 0.9T_c, 1.0T_c$ and $1.1T_c$, respectively. The solid (white) lines represent the light cone. The left subpanel for each T is the result computed by the RPA (2) and (3), while the right one shows the approximate formula (11).

with Eq. (4), and the approximation (11), respectively. One finds that the former is well reproduced by the latter especially at the low energy region at which the soft mode has a significant strength.

Although the spectral properties of the soft mode of the QCD CP look quite similar to that of the diquark soft mode [16], the present $\Xi^R(\mathbf{k},\omega)$ is not analytic at the origin $(|\mathbf{k}|,\omega) = (0,0)$ and it has a discontinuity at the light cone, in contrast to that of the diquark mode; the discontinuity of the diquark propagator coming from the light cone is located at $|\omega + 2\mu| = |\mathbf{k}|$, and accrodingly analytic at the origin [16, 20]. This difference makes the following analysis require some extra caution in the present case.

3 Dilepton production rate and electric conductivity

In this section, we shall calculate the dilepton production rate (DPR) and the electric conductivity assuming that the system is in the vicinity of the QCD CP. In this case, these observables would be significantly modified by the soft modes. Their effects are incorporated through the calculation of the photon self-energy by taking them into account. We perform this analysis in a parallel way to the analysis in Ref. [16] that investigated the diquark soft modes. Once the retarded photon self-energy $\Pi^{R\mu\nu}(\mathbf{k},\omega)$ is obtained, the DPR is calculated to be

$$\frac{d^4\Gamma}{d^4k}(\mathbf{k},\omega) = -\frac{\alpha}{12\pi^4} \frac{1}{k^2} \frac{1}{e^{\omega/T} - 1} g_{\mu\nu} \text{Im} \Pi^{R\mu\nu}(\mathbf{k},\omega), \tag{13}$$

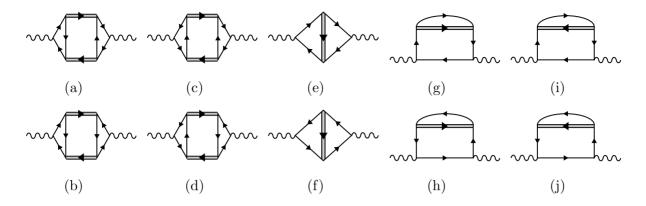


Fig. 3: Diagrammatic representations of the Aslamazov-Larkin (a)–(d), Maki-Thompson (e, f) and density of states (g)–(j) terms with the soft modes. The single, double and wavy lines are quarks, soft modes and photons, respectively.

with the fine structure constant α and the Minkowski metric $g_{\mu\nu}$. The electric conductivity σ is also obtained as [28]

$$\sigma = \frac{1}{3} \lim_{\omega \to 0} \frac{1}{\omega} \sum_{i=1,2,3} \operatorname{Im} \Pi^{Rii}(\mathbf{0}, \omega).$$
 (14)

3.1 Modification of photon self-energy by the soft mode

To construct the photon self-energy in a gauge-invariant way, we start from the lowest-order contribution of the soft mode to the thermodynamic potential $\Omega_{\rm fluc} = \int_p \ln[G_S \tilde{\Xi}^{-1}(p)]$, which is diagrammatically represented by the one-loop graph of the soft mode propagator. The photon self-energy is then constructed by attaching electromagnetic vertices at two points of quark lines in $\Omega_{\rm fluc}$. This procedure leads to ten types of diagrams shown in Fig. 3. By borrowing the nomenclature in the theory of superconductivity [16, 21, 22], we call (a)–(d) the Aslamazov-Larkin (AL) [21], (e) and (f) the Maki-Thompson (MT) [22] and (g)–(j) the density of states (DOS) terms, respectively. The respective contributions to the photon self-energy, $\tilde{\Pi}_{\rm AL}^{\mu\nu}(k)$, $\tilde{\Pi}_{\rm MT}^{\mu\nu}(k)$ and $\tilde{\Pi}_{\rm DOS}^{\mu\nu}(k)$, in the imaginary-time formalism are expressed as

$$\Pi_{\rm AL}^{\mu\nu}(k) = \sum_{f} \int_{q} \tilde{\Gamma}_{f}^{\mu}(q, q+k) \tilde{\Xi}(q+k) \tilde{\Gamma}_{f}^{\nu}(q+k, q) \tilde{\Xi}(q), \tag{15}$$

$$\Pi_{\mathrm{MT}}^{\mu\nu}(k) = \sum_{f} \int_{q} \tilde{\Xi}(q) \mathcal{R}_{\mathrm{MT},f}^{\mu\nu}(q,k), \tag{16}$$

$$\Pi_{\text{DOS}}^{\mu\nu}(k) = \sum_{f} \int_{q} \tilde{\Xi}(q) \mathcal{R}_{\text{DOS},f}^{\mu\nu}(q,k), \tag{17}$$

where f = u, d is the index of flavors and the vertex functions $\tilde{\Gamma}_f^{\mu}(q, q + k)$, $\mathcal{R}_{\text{MT}, f}^{\mu\nu}(q, k)$ and $\mathcal{R}_{\text{DOS}, f}^{\mu\nu}(q, k)$ represent the three- and four-point diagrams in Fig. 3. We note that the number of diagrams is doubled compared with the case in Ref. [16], since the quark and anti-quark lines should be distinguished for the present case.

The total photon self-energy reads

$$\tilde{\Pi}^{\mu\nu}(k) = \tilde{\Pi}^{\mu\nu}_{\text{free}}(k) + \tilde{\Pi}^{\mu\nu}_{\text{fluc}}(k), \tag{18}$$

$$\tilde{\Pi}_{\text{fluc}}^{\mu\nu}(k) = \tilde{\Pi}_{\text{AL}}^{\mu\nu}(k) + \tilde{\Pi}_{\text{MT}}^{\mu\nu}(k) + \tilde{\Pi}_{\text{DOS}}^{\mu\nu}(k), \tag{19}$$

where $\tilde{\Pi}^{\mu\nu}_{\rm fluc}(k)$ is the contribution from the soft modes and

$$\tilde{\Pi}_{\text{free}}^{\mu\nu}(k) = N_c C_{\text{em}} \int_p \text{Tr}[\gamma^{\mu} \mathcal{G}(p+k) \gamma^{\nu} \mathcal{G}(p)], \qquad (20)$$

is the self-energy of the free-quark system, where $C_{\rm em}=e_u^2+e_d^2$ with $e_u=2|e|/3$ ($e_d=-|e|/3$) denoting the electric charges of up (down) quark. We note that $\tilde{\Pi}^{\mu\nu}(k)$ thus constructed nicely satisfies the Ward-Takahashi (WT) identity

$$k_{\mu}\tilde{\Pi}^{\mu\nu}(k) = 0. \tag{21}$$

3.2 Vertices

For the vertex functions $\tilde{\Gamma}_f^{\mu}(q,q+k)$, $\mathcal{R}_{\mathrm{MT},f}^{\mu\nu}(q,k)$ and $\mathcal{R}_{\mathrm{DOS},f}^{\mu\nu}(q,k)$, instead of calculating the diagrams in Fig. 3 directly we determine their functional forms from the WT identities for the vertices

$$k_{\mu}\tilde{\Gamma}_{f}^{\mu}(q,q+k) = -e_{f}[\tilde{\Xi}^{-1}(q+k) - \tilde{\Xi}^{-1}(q)],$$
 (22)

$$k_{\mu} \mathcal{R}_{f}^{\mu\nu}(q,k) = -e_{f} [\tilde{\Gamma}_{f}^{\nu}(q-k,q) - \tilde{\Gamma}_{f}^{\nu}(q,q+k)],$$
 (23)

where $\mathcal{R}^{\mu\nu}(q,k) = \mathcal{R}^{\mu\nu}_{\mathrm{MT},f}(q,k) + \mathcal{R}^{\mu\nu}_{\mathrm{DOS},f}(q,k)$.

Among the vertex functions, only their spatial components are needed for the calculations of Eqs. (13) and (14), because $\tilde{\Pi}_{\text{fluc}}^{00}(k)$ in Eq. (13) is obtained from the spatial components through

$$\tilde{\Pi}^{00}(k) = \frac{\mathbf{k}^2}{(i\nu_l)^2} \tilde{\Pi}^{11}(k) \quad \text{for} \quad k = (|\mathbf{k}|, 0, 0, i\nu_l).$$
(24)

To obtain $\tilde{\Gamma}_f^i(q,q+k)$ for i=1,2,3, we take the same procedure as that adopted in Ref. [16], where the energy dependent and independent terms of $\tilde{\Xi}^{-1}(q)$ on the right-hand

side in Eq. (22) are attributed to $k_0 \tilde{\Gamma}_f^0(q, q + k)$ and $\mathbf{k} \cdot \tilde{\mathbf{\Gamma}}_f(q, q + k)$ on the left-hand side, respectively, so that the spatial part of Eq. (22) is given by ¹

$$\mathbf{k} \cdot \tilde{\mathbf{\Gamma}}_f(q, q+k) = e_f[A(\mathbf{q} + \mathbf{k}) - A(\mathbf{q})]. \tag{25}$$

We then employ the ansatz on the form of $\tilde{\Gamma}_f^i(q,q+k)$ that satisfies Eq. (25) as

$$\tilde{\Gamma}_f^i(q, q+k) = e_f Q_{(1)}(\boldsymbol{q} + \boldsymbol{k}, \boldsymbol{q})(2q+k)^i, \tag{26}$$

$$Q_{(1)}(\mathbf{q}_1, \mathbf{q}_2) = \frac{A(\mathbf{q}_1) - A(\mathbf{q}_2)}{|\mathbf{q}_1|^2 - |\mathbf{q}_2|^2}.$$
 (27)

Since A(q) is real, $\tilde{\Gamma}_f^i(q, q + k)$ is also a real function in this construction. We note that this form of approximation is valid only for sufficiently small k, as the WT identity (22) cannot uniquely determine the vertex in general. Near the QCD CP at which the contribution of the soft mode becomes prominent, it is, however, expected that the qualitative result does not depend on the form of the vertex and our approximation would be well justified.

The form of the vertex $\mathcal{R}_f^{ij}(q,k)$ is also obtained by adopting a similar argument with Eqs. (23) and (26), as was done in Ref. [16]. From this analysis it is found that $\mathcal{R}_f^{ij}(q,k)$ is a real function and independent of $i\nu_l$. By constructing the MT and DOS terms from the vertex, one finds

$$\operatorname{Im}\Pi_{\mathrm{MT}}^{Rij}(\boldsymbol{k},\omega) + \operatorname{Im}\Pi_{\mathrm{DOS}}^{Rij}(\boldsymbol{k},\omega) = 0.$$
 (28)

Equation (28) is shown from the fact that the sum of Eqs. (16) and (17) becomes real after the Matsubara summations when $\mathcal{R}_f^{ij}(q,k)$ satisfies the above conditions [16, 29]. The cancellation of the MT and DOS terms is also known in metallic superconductivity [24].

From Eqs. (28) and (24), one obtains

$$\operatorname{Im}\Pi_{\text{fluc}}^{R00}(\boldsymbol{k},\omega) = \frac{\boldsymbol{k}^2}{\omega^2} \operatorname{Im}\Pi_{\text{AL}}^{R11}(\boldsymbol{k},\omega) \quad \text{for} \quad \boldsymbol{k} = (|\boldsymbol{k}|, 0, 0).$$
 (29)

Plugging this into Eq. (13), one finds that the DPR is written solely in terms of the AL term. So is the electric conductivity since it is given by the spatial components of $\text{Im}\Pi_{\text{fluc}}^{R\mu\nu}(\mathbf{k},\omega)$ as in Eq. (14). These results show that we only have to compute the AL term for obtaining both the DPR and the electric conductivity.

This procedure is justified by calculating $\tilde{\Gamma}_f^{\mu}(q, q + k)$ from the triangle diagrams in Fig. 3 (a)–(d) directly and comparing the functional forms in the small ω and k limit [29].

3.3 Aslamazov-Larkin term

Since $\text{Im}\tilde{\Pi}^{ij}_{\text{fluc}}(k)$ consists of only the AL term, we now calculate $\tilde{\Pi}^{ij}_{\text{AL}}(k)$. Using Eqs. (11) and (26), we obtain

$$\tilde{\Pi}_{AL}^{ij}(k) = \sum_{f} \int \frac{d^3 \mathbf{q}}{(2\pi)^3} \tilde{\Gamma}_f^i(q, q+k) \tilde{\Gamma}_f^j(q+k, q) \oint_C \frac{dq_0}{2\pi i} \frac{\coth\frac{q_0}{2T}}{2} \tilde{\Xi}(q+k) \tilde{\Xi}(q), \quad (30)$$

where the contour C encircles the imaginary axis, which is deformed so as to avoid the cut in $\tilde{\Xi}(q+k)$ and $\tilde{\Xi}(q)$.

Taking the analytic continuation $i\nu_l \to \omega + i\eta$ and using Eq. (29) we obtain

$$g_{\mu\nu}\operatorname{Im}\Pi_{\mathrm{fluc}}^{R\mu\nu}(\boldsymbol{k},\omega) = \frac{\boldsymbol{k}^{2}}{\omega^{2}}\operatorname{Im}\Pi_{\mathrm{AL}}^{R11}(\boldsymbol{k},\omega) - \sum_{i}\operatorname{Im}\Pi_{\mathrm{AL}}^{Rii}(\boldsymbol{k},\omega)$$

$$= C_{\mathrm{em}} \int \frac{d^{3}\boldsymbol{q}}{(2\pi)^{3}} \int \frac{d\omega'}{2\pi} \operatorname{coth} \frac{\omega'}{2T}$$

$$\times \left(Q_{(1)}(\boldsymbol{q}+\boldsymbol{k},\boldsymbol{q})\right)^{2} \left[\left(\frac{(\boldsymbol{q}+\boldsymbol{k})^{2}-\boldsymbol{q}^{2}}{\omega}\right)^{2} - (2\boldsymbol{q}+\boldsymbol{k})^{2}\right]$$

$$\times \operatorname{Im}\Xi^{R}(\boldsymbol{q}+\boldsymbol{k},\omega') \left\{\operatorname{Im}\Xi^{R}(\boldsymbol{q},\omega'+\omega) - \operatorname{Im}\Xi^{R}(\boldsymbol{q},\omega'-\omega)\right\}. \tag{31}$$

The contribution of the soft mode to the DPR is computed by substituting Eq. (31) into Eq. (13). The contribution of the soft mode to the electric conductivity is also obtained by plugging the formula

$$\sum_{i=1}^{3} \operatorname{Im}\Pi_{\text{fluc}}^{Rii}(\boldsymbol{k},\omega) = C_{\text{em}} \int \frac{d^{3}\boldsymbol{q}}{(2\pi)^{3}} \int \frac{d\omega'}{2\pi} \coth\frac{\omega'}{2T} \left(Q_{(1)}(\boldsymbol{q}+\boldsymbol{k},\boldsymbol{q})\right)^{2} (2\boldsymbol{q}+\boldsymbol{k})^{2} \times \operatorname{Im}\Xi^{R}(\boldsymbol{q}+\boldsymbol{k},\omega') \left\{ \operatorname{Im}\Xi^{R}(\boldsymbol{q},\omega'+\omega) - \operatorname{Im}\Xi^{R}(\boldsymbol{q},\omega'-\omega) \right\},$$
(32)

into Eq. (14). We note that Eq. (32) at $|\mathbf{k}| = 0$ is linearly dependent on ω in the $\omega \to 0$ limit, and hence the conductivity σ calculated from it has a nonzero value. This term leads to the divergence of σ at the QCD CP as we will see in the next section.

We note that the domain of the integral in Eq. (31) or (32) is subject to a constraint that Eq. (11) takes a nonzero value only in the energy-momentum region $|\omega| < \bar{k}(|\mathbf{k}|, \bar{\Lambda})$, i.e., inside the space-like region. Nevertheless, we note that some multiple soft mode processes can affect the photon self-energy in the time-like region that is responsible for the DPR and conductivity. These contributions are understood as the scattering process of the photon with a soft mode: Let a virtual photon with the energy-momentum $k = (\mathbf{k}, \omega)$ is absorbed by a soft mode with $q_1 = (\mathbf{q}_1, \omega_1)$ to make another one with $q_2 = (\mathbf{q}_2, \omega_2)$, both of which are in the space-like region; $|\omega_1| < |\mathbf{q}_1|$ and $|\omega_2| < |\mathbf{q}_2|$. Then, the energy-momentum conservation law

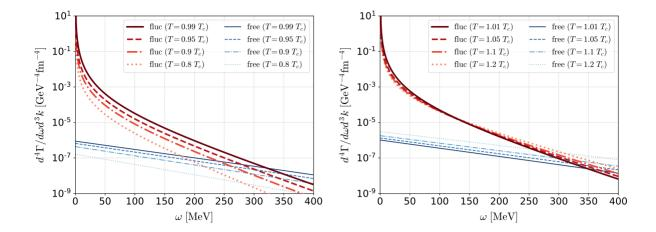


Fig. 4: Dilepton production rate (DPR) per unit energy and momentum $d^4\Gamma/d\omega d^3k$ for several values of T/T_c at $\mu = \mu_c$ and $\mathbf{k} = \mathbf{0}$. The thick (red) and thin (blue) lines are the contributions from the soft mode and the massless quark gases, respectively. The left and right panels show the DPR below and above T_c , respectively.

tells us that $\mathbf{k} = \mathbf{q}_2 - \mathbf{q}_1$ and $\omega = \omega_2 - \omega_1$, where $|\mathbf{k}|$ can be taken arbitrarily small keeping $\omega = \omega_2 - \omega_1$ finite. Thus, the soft mode which has the spectral support in the space-like region can contribute to the photon self-energy in the time-like region ($\omega > |\mathbf{k}|$). In the next section we shall see that it can cause an enhancement of the DPR and conductivity.

Before closing this section, let us clarify the limitation of our calculation. Firstly, in our treatment we focus on the effects of the soft mode in the space-like region, and the effects of the mesonic mode in the time-like region is neglected. This approximation is justified as long as we consider the DPR in the low energy region near the QCD CP, since the mass of the sigma mode is larger than $2M \simeq 370$ MeV. When considering the DPR above 2M, however, the effect of the mesonic modes will become significant. Secondly, we have constructed the approximate forms of the vertex functions through the WT identities and Eq. (10). While this assumption should be valid for sufficiently small ω , it would not be directly applicable to the large energy-momentum region.

4 Numerical results

In this section, we shall show the numerical results of the DPR (13) and electric conductivity (14) near the QCD CP calculated with the photon self-energy obtained in the previous section.

We first show the DPR at $\mathbf{k} = \mathbf{0}$ at $\mu = \mu_c$ for several values of T below (above) T_c in the left (right) panel of Fig. 4. The red-thick lines show the contribution from $\tilde{\Pi}_{\text{fluc}}^{\mu\nu}(k)$. The total

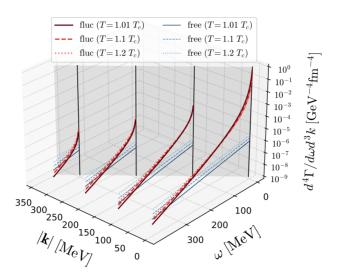


Fig. 5: DPR $d^4\Gamma/d\omega d^3k$ with the finite momentum k for $T/T_c=1.01, 1.1$ and 1.2 at $\mu=\mu_c$. The gray surface shows the light-cone.

rate is given by the sum of the contributions from $\tilde{\Pi}^{\mu\nu}_{\mathrm{flue}}(k)$ and $\tilde{\Pi}^{\mu\nu}_{\mathrm{free}}(k)$. However, the latter is almost negligible at the QCD CP in the range of ω in the figure since $\mathrm{Im}\tilde{\Pi}^{\mu\nu}_{\mathrm{free}}(k)$ has a nonzero value only for $|\omega| > \sqrt{k^2 + 4M^2}$, where $M \simeq 185$ MeV at the QCD CP. For a comparison, the DPR from the massless free-quark gas are shown by the blue-thin lines in the figure. The figure shows that the DPR is enhanced significantly near the QCD CP by the soft modes and well exceeds the case of the massless free-quark gas in the low energy region $\omega \lesssim 250$ MeV. The enhancement in the low energy region becomes more prominent as T approaches T_c from both sides of the temperature. Taking a closer look at these results, one finds that the DPR increases monotonically in the left panel as T approaches T_c , while the T dependence for $T > T_c$ shown in the right panel is not monotonous. The latter can be accounted for by a competition of the effect of the soft modes and the kinematical temperature effect causing more thermal excitations of the soft modes at higher temperatures. Figure 5 shows the numerical results of the DPR at nonzero momentum for several T above T_c . One finds that the enhancement of the DPR is more prominent in the low-momentum region.

In the HIC experiments, the DPR is usually observed as a function of the invariant-mass m_{ll} ,

$$\frac{d\Gamma}{dm_{ll}^2} = \int d^3k \frac{1}{2\omega} \frac{d^4\Gamma}{d^4k} \bigg|_{\omega = \sqrt{\mathbf{k}^2 + m_{ll}^2}},\tag{33}$$

to cancel out the effect of the flow. In Fig. 6, we show the numerical results of Eq. (33) for various values of T at $\mu = \mu_c$. We find that the contribution of the soft modes is conspicuous in the low invariant-mass region $m_{ll} \lesssim 150$ MeV.

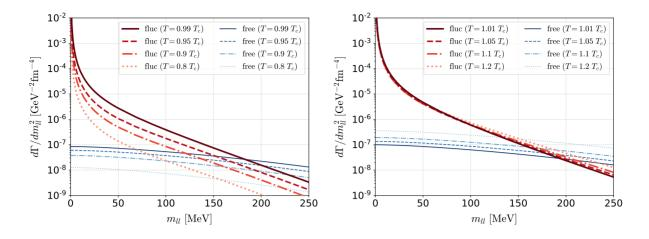


Fig. 6: Invariant-mass spectrum $d\Gamma/dm_{ll}^2$ at $\mu = \mu_c$. Left: For $T/T_c = 0.8, 0.9, 0.95$ and 0.99. Right: For $T/T_c = 1.01, 1.05, 1.1$ and 1.20.

Finally, we show the behavior of the electric conductivity σ near the QCD CP in Fig. 7. The left panel is the T dependence of σ at three values of μ , where σ is normalized by $TC_{\rm em}$. As expected from the infrared behavior of the soft modes in the critical region, the conductivity σ tends to diverge near the CP. In fact, it can be shown that σ grows as $|T - T_c|^{-2/3}$ in the vicinity of the critical point in the present approximation, as will be discussed in detail in the forthcoming publication [29]. At $\mu = 0.99 \,\mu_c$, the conductivity is not divergent but only shows a prominent but finite peak at $T \simeq 1.08 \, T_c$ in accordance with the crossover nature of the transition. At $\mu = 1.01 \,\mu_c$, the σ shows a cusp-like behavior reflecting the first-order nature of the phase transition at $T \simeq 0.9 \, T_c$. The right panel of Fig. 7 shows a contour plot of $\sigma/TC_{\rm em}$ on the T- μ plane. One sees that the σ has a significant excess along the critical lines of the first-order phase and crossover transitions.

5 Discussions

Focusing on the collective soft modes the mass of which tends to vanish at the QCD CP, we have explored its effects on the dilepton production rate (DPR) and the electric conductivity near the QCD CP. The contribution to these observables was taken into account through the modification of the photon self-energy by the AL, MT and DOS terms, the inclusion of all of which is necessary to assure the WT identity. We have shown that the DPR in the low energy and low invariant-mass regions is greatly enhanced due to the soft modes around the CP in comparison with that of the massless free-quark gas. We have also seen that the prominent enhancement of the electric conductivity σ occurs near the QCD CP due to the soft modes. We plan to report on more detailed analyses on the possible

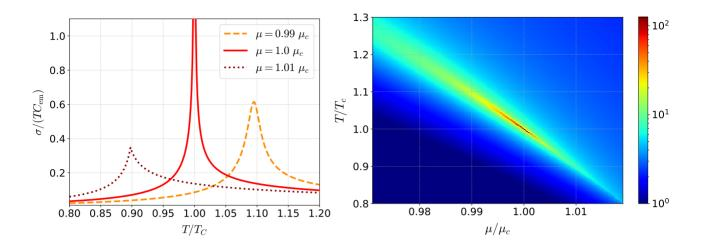


Fig. 7: Electric conductivity σ associated with the soft modes. **Left**: T dependence of the σ . The results of $\mu/\mu_c = 0.99$, 1.0 and 1.01 are the dashed, solid and dotted lines, repectively. **Right**: Contour plot of σ in the T- μ plane around the QCD CP.

anomalous transport properties including the electric conductivity and relaxation time near the QCD CP, as well as the phase boundary of the 2SC phase, elsewhere [29].

It is interesting to explore the phenomenological consequence of the present findings in the HIC experiments. If an anomalous enhancement of the DPR in the low mass region, say less than 150 MeV, should ever be detected, our result suggests that it may be the signal of the QCD CP. The enhancement of the conductivity at the CP will also be observed in the HIC [30]. To identify the signal, however, it is important to disentangle the signal from other effects that induces a similar enhancement. For example, in our previous study we have pointed out that a similar enhancement of the DPR manifests itself near the phase boundary of the 2SC phase due to the development of the diquark soft modes [29]. Other standard mechanisms due to medium effects, such as hadronic scenarios and the processes to be described by the perturbative QCD and so on [31–33], also bring about the enhancement at low mass region. More detailed investigation of the invariant-mass spectrum of the DPR will be required to disentangle these effects.

Other important issues to be examined are the effects of dynamics. In the dynamical evolution of the HIC, the effect of the critical slowing down will modify the DPR around the QCD CP. To deal with this effect, the analysis of the DPR in the real-time formalism with the time-dependent background medium is required. It will also be important to understand the effects of the phase transitions on the bulk evolution of the medium [34]. For elucidating the production mechanisms and the respective characteristics, one would eventually need to recourse to some dynamical transport models [35–38]. These investigations are left for future

study. Nevertheless, we would like to emphasize that the production mechanism of the DPR through the soft modes is robust.

The measurements of the DPR in the low invariant-mass region $m_{ll} \lesssim 100-200$ MeV is also a challenge in the experimental side, because di-electrons are contaminated by the Dalitz decay in this energy region. In spite of these challenging demands, however, it is encouraging that the future HIC programs in GSI and J-PARC-HI are designed to carry out high-statistical experiments [9–11], and also that new technical developments are vigorously being made [30].

Finally, we remark that a complete description of the collective soft modes around the QCD CP needs to incorporate the vector coupling [39, 40] as well as the scalar couplings which was exclusively taken into account in the present study. Such a more complete analyses constitutes one of the future tasks, which we hope to report somewhere in future.

Acknowledgements

The authors thank Berndt Mueller, Hirotsugu Fujii and Akira Ohnishi for valuable comments. T. N. thanks JST SPRING (Grant No. JPMJSP2138) and Multidisciplinary PhD Program for Pioneering Quantum Beam Application. This work was supported by JSPS KAKENHI (Grants No. JP19K03872, No. JP19H05598, No. 20H01903, No. 22K03619).

References

- A. Lovato, et al., Long Range Plan: Dense matter theory for heavy-ion collisions and neutron stars (11 2022).
 arXiv: 2211.02224.
- M. A. Stephanov, K. Rajagopal, E. V. Shuryak, Signatures of the tricritical point in QCD, Phys. Rev. Lett. 81 (1998) 4816-4819. arXiv:hep-ph/9806219, doi:10.1103/PhysRevLett.81.4816.
- [3] M. A. Stephanov, K. Rajagopal, E. V. Shuryak, Event-by-event fluctuations in heavy ion collisions and the QCD critical point, Phys. Rev. D 60 (1999) 114028. arXiv:hep-ph/9903292, doi:10.1103/PhysRevD.60.114028.
- [4] Y. Hatta, M. A. Stephanov, Proton number fluctuation as a signal of the QCD critical endpoint, Phys. Rev. Lett. 91 (2003) 102003, [Erratum: Phys.Rev.Lett. 91, 129901 (2003)]. arXiv:hep-ph/0302002, doi:10.1103/PhysRevLett.91.102003.
- [5] Y. Minami, T. Kunihiro, Dynamical Density Fluctuations around QCD Critical Point Based on Dissipative Relativistic Fluid Dynamics -Possible fate of Mach cone at the critical point-, Prog. Theor. Phys. 122 (2010) 881–910. arXiv:0904.2270, doi:10.1143/PTP.122.881.
- [6] M. Asakawa, S. Ejiri, M. Kitazawa, Third moments of conserved charges as probes of QCD phase structure, Phys. Rev. Lett. 103 (2009) 262301. arXiv:0904.2089, doi:10.1103/PhysRevLett.103.262301.
- [7] M. Asakawa, M. Kitazawa, Fluctuations of conserved charges in relativistic heavy ion collisions: An introduction, Prog. Part. Nucl. Phys. 90 (2016) 299-342. arXiv:1512.05038, doi:10.1016/j.ppnp.2016.04.002.
- [8] M. Hasanujjaman, G. Sarwar, M. Rahaman, A. Bhattacharyya, J.-e. Alam, Dynamical spectral structure of density fluctuation near the QCD critical point, Eur. Phys. J. A 57 (10) (2021) 283. arXiv:2008.03931, doi:10.1140/epja/s10050-021-00589-3.
- [9] T. Galatyuk, Future facilities for high μ_B physics, Nucl. Phys. A 982 (2019) 163–169. doi:10.1016/j.nuclphysa.2018.11.025.
- [10] K. Agarwal, Status of the Compressed Baryonic Matter (CBM) Experiment at FAIR, Acta Phys. Polon. Supp. 16 (2023) 1–A142. arXiv:2207.14585, doi:10.5506/aphyspolbsupp.16.1-a142.
- [11] K. Ozawa, et al., The J-PARC heavy ion project, EPJ Web Conf. 271 (2022) 11004. doi:10.1051/epjconf/ 202227111004.

- [12] H. Fujii, M. Ohtani, Sigma and hydrodynamic modes along the critical line, Phys. Rev. D 70 (2004) 014016. arXiv:hep-ph/0402263, doi:10.1103/PhysRevD.70.014016.
- [13] D. T. Son, M. A. Stephanov, Dynamic universality class of the QCD critical point, Phys. Rev. D 70 (2004) 056001. arXiv:hep-ph/0401052, doi:10.1103/PhysRevD.70.056001.
- [14] T. Yokota, T. Kunihiro, K. Morita, Functional renormalization group analysis of the soft mode at the QCD critical point, PTEP 2016 (7) (2016) 073D01. arXiv:1603.02147, doi:10.1093/ptep/ptw062.
- [15] T. Yokota, T. Kunihiro, K. Morita, Tachyonic instability of the scalar mode prior to the QCD critical point based on the functional renormalization-group method in the two-flavor case, Phys. Rev. D 96 (7) (2017) 074028. arXiv:1707.05520, doi:10.1103/PhysRevD.96.074028.
- [16] T. Nishimura, M. Kitazawa, T. Kunihiro, Anomalous enhancement of dilepton production as a precursor of color superconductivity, PTEP 2022 (9) (2022) 093D02. arXiv:2201.01963, doi:10.1093/ptep/ptac100.
- [17] D. N. Voskresensky, Fluctuations of the color superconducting order parameter in heated and dense quark matter (6 2003). arXiv:nucl-th/0306077.
- [18] M. Kitazawa, T. Koide, T. Kunihiro, Y. Nemoto, Precursor of color superconductivity in hot quark matter, Phys. Rev. D 65 (2002) 091504. arXiv:nucl-th/0111022, doi:10.1103/PhysRevD.65.091504.
- [19] M. Kitazawa, T. Koide, T. Kunihiro, Y. Nemoto, Pseudogap of color superconductivity in heated quark matter, Phys. Rev. D 70 (2004) 056003. arXiv:hep-ph/0309026, doi:10.1103/PhysRevD.70.056003.
- [20] M. Kitazawa, T. Koide, T. Kunihiro, Y. Nemoto, Pre-critical phenomena of two-flavor color superconductivity in heated quark matter: Diquark-pair fluctuations and non-Fermi liquid behavior, Prog. Theor. Phys. 114 (2005) 117-155. arXiv:hep-ph/0502035, doi:10.1143/PTP.114.117.
- [21] L. Aslamazov, A. Larkin, Soviet solid state 10, 875 (1968), Phys. Lett. A 26 (1968) 238.
- [22] K. Maki, Critical fluctuation of the order parameter in a superconductor. I, Progress of Theoretical Physics 40 (2) (1968) 193–200.
- [23] R. S. Thompson, Microwave, flux flow, and fluctuation resistance of dirty type-II superconductors, Physical Review B 1 (1) (1970) 327.
- [24] A. Larkin, A. Varlamov, Fluctuation phenomena in superconductors, Springer, 2008.
- [25] T. Hatsuda, T. Kunihiro, QCD phenomenology based on a chiral effective Lagrangian, Phys. Rept. 247 (1994) 221–367. arXiv:hep-ph/9401310, doi:10.1016/0370-1573(94)90022-1.
- [26] H. Fujii, Scalar density fluctuation at critical end point in NJL model, Phys. Rev. D 67 (2003) 094018. arXiv: hep-ph/0302167, doi:10.1103/PhysRevD.67.094018.
- [27] D. J. Thouless, Perturbation theory in statistical mechanics and the theory of superconductivity, Annals of Physics 10 (4) (1960) 553–588.
- [28] J. I. Kapusta, C. Gale, Finite-temperature field theory: Principles and applications, Cambridge Monographs on Mathematical Physics, Cambridge University Press, 2011. doi:10.1017/CB09780511535130.
- [29] T. Nishimura, M. Kitazawa, T. Kunihiro, in preparation.
- [30] D. Adamová, et al., A next-generation LHC heavy-ion experiment (1 2019). arXiv:1902.01211.
- [31] R. Rapp, J. Wambach, H. van Hees, The Chiral Restoration Transition of QCD and Low Mass Dileptons, Landolt-Bornstein 23 (2010) 134. arXiv:0901.3289, doi:10.1007/978-3-642-01539-7_6.
- [32] M. Laine, NLO thermal dilepton rate at non-zero momentum, JHEP 11 (2013) 120. arXiv:1310.0164, doi: 10.1007/JHEP11(2013)120.
- [33] J. Ghiglieri, G. D. Moore, Low Mass Thermal Dilepton Production at NLO in a Weakly Coupled Quark-Gluon Plasma, JHEP 12 (2014) 029. arXiv:1410.4203, doi:10.1007/JHEP12(2014)029.
- [34] O. Savchuk, A. Motornenko, J. Steinheimer, V. Vovchenko, M. Bleicher, M. Gorenstein, T. Galatyuk, Enhanced dilepton emission from a phase transition in dense matter (9 2022). arXiv: 2209.05267.
- [35] S. A. Bass, et al., Microscopic models for ultrarelativistic heavy ion collisions, Prog. Part. Nucl. Phys. 41 (1998) 255–369. arXiv:nucl-th/9803035, doi:10.1016/S0146-6410(98)00058-1.
- [36] J. Weil, et al., Particle production and equilibrium properties within a new hadron transport approach for heavyion collisions, Phys. Rev. C 94 (5) (2016) 054905. arXiv:1606.06642, doi:10.1103/PhysRevC.94.054905.
- [37] Y. Akamatsu, M. Asakawa, T. Hirano, M. Kitazawa, K. Morita, K. Murase, Y. Nara, C. Nonaka, A. Ohnishi, Dynamically integrated transport approach for heavy-ion collisions at high baryon density, Phys. Rev. C 98 (2) (2018) 024909. arXiv:1805.09024, doi:10.1103/PhysRevC.98.024909.
- [38] Y. Nara, A. Ohnishi, JAM mean-field update: mean-field effects on collective flow in high-energy heavy-ion collisions at $\sqrt{s_{NN}} = 2 20$ GeV energies (9 2021). arXiv:2109.07594.
- [39] T. Kunihiro, Quark number susceptibility and fluctuations in the vector channel at high temperatures, Phys. Lett. B 271 (1991) 395–402. doi:10.1016/0370-2693(91)90107-2.
- [40] M. Kitazawa, T. Koide, T. Kunihiro, Y. Nemoto, Chiral and color superconducting phase transitions with vector interaction in a simple model, Prog. Theor. Phys. 108 (5) (2002) 929–951, [Erratum: Prog.Theor.Phys. 110, 185–186 (2003)]. arXiv:hep-ph/0207255, doi:10.1143/PTP.108.929.